Geophysical Prospecting
EAGE EUROPEAN ASSOCIATION OF GEOSCIENTISTS & ENGINEERS
Geophysical Prospecting, 2021, **69**, 269–288 doi: 10.1111/1365-2478.13051

Kirchhoff pre-stack depth scalar migration in a simple triclinic velocity model for three-component P, S1, S2 and converted waves

Václav Bucha*

Department of Geophysics, Faculty of Mathematics and Physics, Charles University, Ke Karlovu 3, 12116 Prague 2, Czech Republic

Received May 2020

ABSTRACT

Migration of multi-component elastic data in anisotropic models is difficult and has not been reasonably addressed. Thus we test three-dimensional ray-based Kirchhoff pre-stack depth scalar migration and calculate migrated sections in a simple anisotropic velocity model. We generate ray-theory seismograms for separate phases of reflected P, S1, S2 and converted waves. The velocity model is composed of two homogeneous layers and one curved interface. The anisotropy of the upper layer is triclinic and the bottom layer is isotropic. We apply a scalar imaging separately to each component of the elementary wave in a single-layer velocity model with the same triclinic anisotropy as in the upper layer of the velocity model used to calculate the recorded wave field. Results of Kirchhoff pre-stack depth scalar migration indicate big differences for individual elementary wave components. We observe very good migrated interface for all three components of reflected PP wave, radial component of PS1 converted wave and transversal component of PS2 converted wave. For other components and elementary waves, the migrated interface is imaged, only partially, correctly.

Key words: Anisotropic velocity model, Triclinic anisotropy, Elastic waves, Three-component seismograms, 3D Kirchhoff pre-stack depth scalar migration.

INTRODUCTION

There are two basic families of pre-stack depth migrations of multi-component seismic data: scalar migration and elastic migration (Hou and Marfurt, 2002). Under the scalar migration type, we often migrate a single seismogram component using the scalar ray-theory amplitude instead of the vectorial ray-theory amplitude. From another point of view, migration of multi-component data has been attempted using either ray-based or wave-based solutions (Wang and McMechan, 2016). Different migration approaches have their own advantages, disadvantages and limitations (e.g. Gray *et al.*, 2001).

The acoustic Kirchhoff migration method is very popular in the industrial world because of its high computational efficiency and flexible imaging while the elastic Kirchhoff migration method is developing slowly (Qizhen and Bo, 2008). Kuo and Dai (1984) and Qizhen and Bo (2008) presented pre-stack elastic Kirchhoff migration in two-dimensional isotropic elastic media for reflected PP and converted PS waves. Hokstad (2000) derived equations for elastic and viscoelastic Kirchhoff migration of multi-component seismic data. However, the theory requires complete boundary conditions on the receiver side, that is, measurement of both displacement and traction (pressure) that is rare in seismic experiments. Hokstad (2000) implemented the method for imaging of marine multi-component seismic data in 2D horizontally layered anisotropic velocity models for reflected PP, SS and converted PS waves.

In this paper, we continue with the three-dimensional ray-based Kirchhoff pre-stack depth scalar migration studies (Bucha, 2012, 2013, 2017). Although the previous studies were limited to the vertical component of P waves, in this

*E-mail: bucha@seis.karlov.mff.cuni.cz

© 2020 European Association of Geoscientists & Engineers

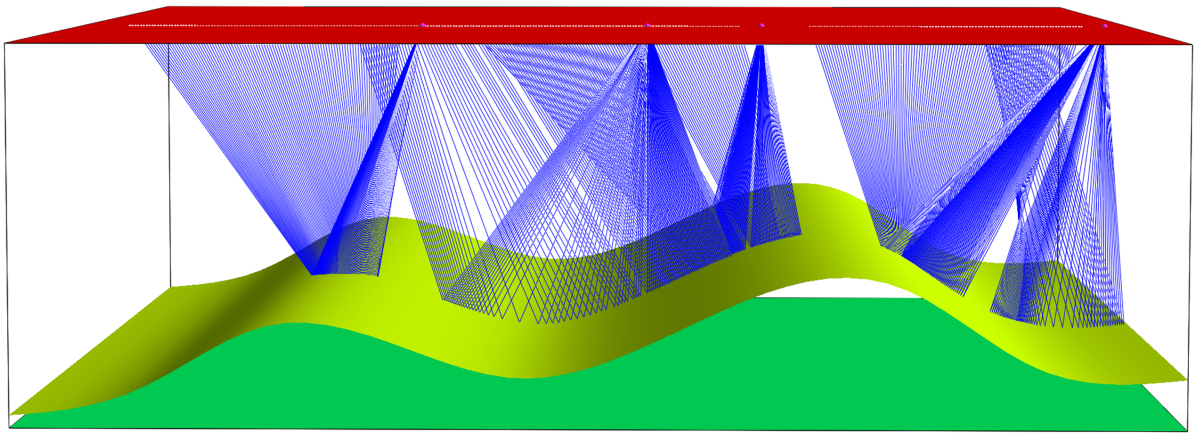

Figure 1 Velocity model with a curved interface and with triclinic anisotropy in the upper layer. The horizontal dimensions of the velocity model are 0 km $\leq x_1 \leq$ 9.2 km, 0 km $\leq x_2 \leq$ 10 km and the depth is 0 km $\leq x_3 \leq$ 3 km. The velocity model contains one curved interface which is non-inclined in the direction perpendicular to the source–receiver profiles. Two-point rays of the converted PS1 wave for one selected profile line (at horizontal coordinate $x_2 = 6$ km) and four shot-receiver configurations (from the left-hand side: shots 1, 80, 120 and 240 along the profile) are displayed.

paper, we use three-component ray-theory P, S1, S2 and converted waves. Main advantages of the ray-theory method are separate calculation of selected elementary waves and low computational cost. However, ray calculations are problematic when singularities and triplications occur.

The dimensions of the velocity model, shot-receiver configuration, methods for calculation of the recorded wave field and the migration are the same as in the previous papers by Bucha (2012, 2013, 2017), where we studied the sensitivity of the migrated images to incorrect anisotropy, to incorrect gradients of elastic moduli or to incorrect rotation of the tensor of elastic moduli (stiffness tensor). Neglecting anisotropy can lead to an incorrect structural interpretation (e.g. Alkhalifah and Larner, 1994; Gray, *et al.*, 2001; Alkhalifah, 2006).

We generate three-component synthetic seismograms of individual reflected P, S1, S2 and converted waves (nine elementary waves) using ray theory, which is approximate. We apply the ANRAY software package (Gajewski and Pšenčík, 1990). We consider radial, transversal and vertical components. To compute the synthetic recorded wave field, we use simple anisotropic velocity model composed of two homogeneous layers separated by one curved interface that is non-inclined in the direction perpendicular to the source–receiver profiles. The anisotropy in the upper layer is triclinic and is thus not mirror symmetric. The complexity of the anisotropy is obvious from the generated and displayed slowness and ray-velocity surfaces of P, S1 and S2 waves. The bottom layer is isotropic.

We then migrate separately individual components of the elementary waves using 3D ray-based Kirchhoff pre-stack depth scalar migration in the single-layer triclinic velocity model. The elastic moduli in the velocity model correspond to the upper layer of the velocity model in which the synthetic seismograms have been calculated. For migration, we utilize MODEL, CRT, FORMS and DATA software packages (Červený *et al.*, 1988; Bulant 1996; Bucha and Bulant 2019). The packages used for calculation of the recorded wave field and for the migration are independent.

ANISOTROPIC VELOCITY MODEL

The dimensions of the velocity model and the measurement configuration are derived from the two-dimensional Marmousi model and dataset (Versteeg and Grau, 1991). The recorded wave field is computed in the velocity model composed of two homogeneous layers separated by one curved interface (see Fig. 1). The medium in the upper layer is triclinic and the bottom layer is isotropic.

The triclinic medium is represented by dry Vosges sandstone (Mensch and Rasolofosaon, 1997). Triclinic anisotropy is asymmetric, there are no mirror planes and no axes of symmetry. The matrix of density-reduced elastic moduli in km^2/s^2 reads

$$\begin{pmatrix} 10.3 & 0.9 & 1.3 & 1.4 & 1.1 & 0.8 \\ & 10.6 & 2.1 & 0.2 & -0.2 & -0.6 \\ & & 14.1 & 0.0 & -0.5 & -1.0 \\ & & & 5.1 & 0.0 & 0.2 \\ & & & & 6.0 & 0.0 \\ & & & & & 4.9 \end{pmatrix}. \quad (1)$$

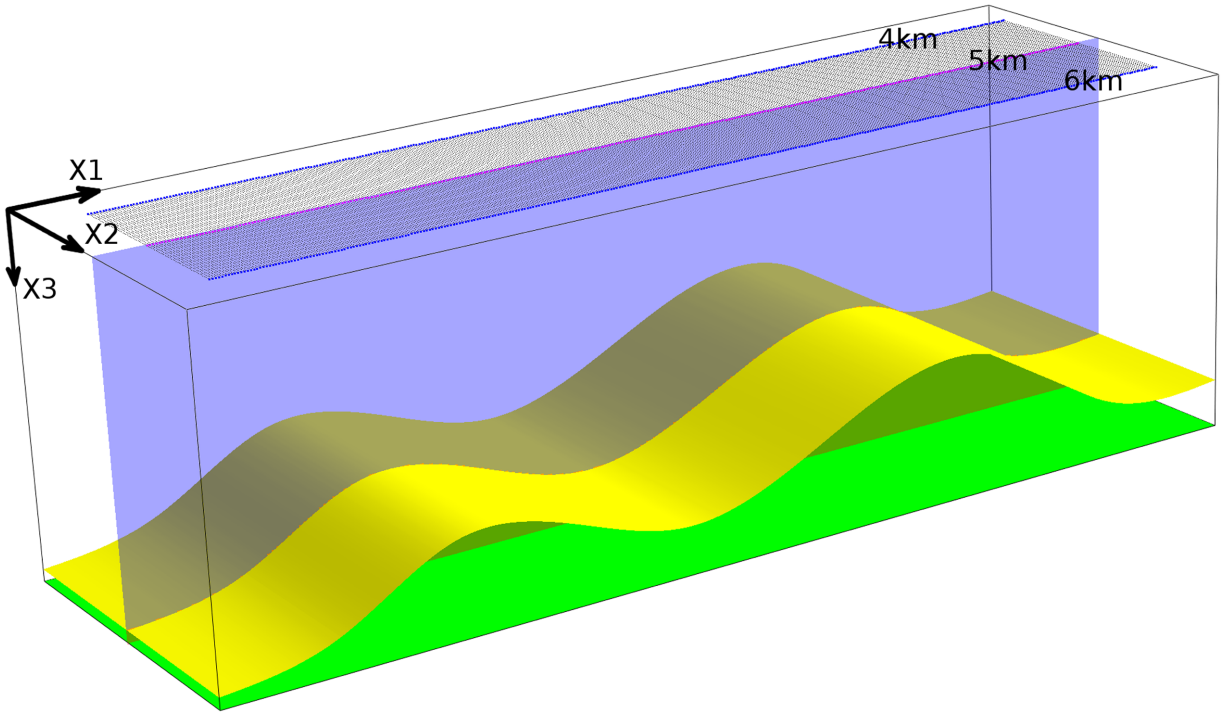

Figure 2 Part of the velocity model with 81 parallel profile lines, the curved interface (yellow) and the bottom velocity model plane (green). We compute and stack migrated sections in the 2D plane (blue) located in the middle of the shot-receiver configuration, at horizontal coordinate $x_2 = 5$ km.

The values of anisotropy strength, defined as $2(P_{\max} - P_{\min})/(P_{\max} + P_{\min}) \times 100\%$, where $P_{\min}$ and $P_{\max}$ are minimum and maximum absolute norms of the slowness vector, are 21.2% for P wave, 17.0% for S1 wave and 19.7% for S2 wave. The P wave velocity in the isotropic bottom layer is $V_p = 3.6$ km/s and the S wave velocity is $V_s = V_p/\sqrt{3}$.

We migrate in the single-layer velocity model (without the interface) with the same triclinic anisotropy given by matrix (1). The elastic moduli in the velocity model correspond to the upper layer of the velocity model in which the synthetic data have been calculated.

SHOTS AND RECEIVERS

The profile lines are parallel with the x_1 coordinate axis (see Figs 1 and 2). Each profile line has the following configuration: The first shot is 3 km from the left-hand side of the velocity model, the last shot is 8.975 km from the left-hand side of the velocity model, the distance between the shots is 0.025 km, and the depth of the shots is 0 km. The total number of shots along one profile line is 240. The number of receivers per shot is 96, the first receiver is located 2.575 km left of the shot location, the last receiver is 0.2 km left of the shot location, the distance between the receivers is 0.025 km, and the depth of the receivers is 0 km. This configuration simulates a simplified towed streamer acquisition geometry. The three-dimensional measurement configuration consists of 81 parallel profile lines (see Fig. 2). The interval between the parallel profile lines is 0.025 km.

RECORDED WAVE FIELD

The recorded wave field in the two-layer velocity model was computed using the ANRAY software package (Gajewski and Pšenčík, 1990). Three-dimensional ray tracing is used to calculate the two-point rays of the reflected P, S1, S2 and converted waves (nine elementary waves). In this paper, we refer to the faster S wave as the S1 wave, and to the slower S wave as the S2 wave. We then compute three-component ray-theory seismograms at the receivers.

The recorded wave field is equal for all parallel profile lines, because the distribution of elastic moduli in each layer is homogeneous, and the non-inclined curved interface is independent of the coordinate x_2 perpendicular to the profile lines

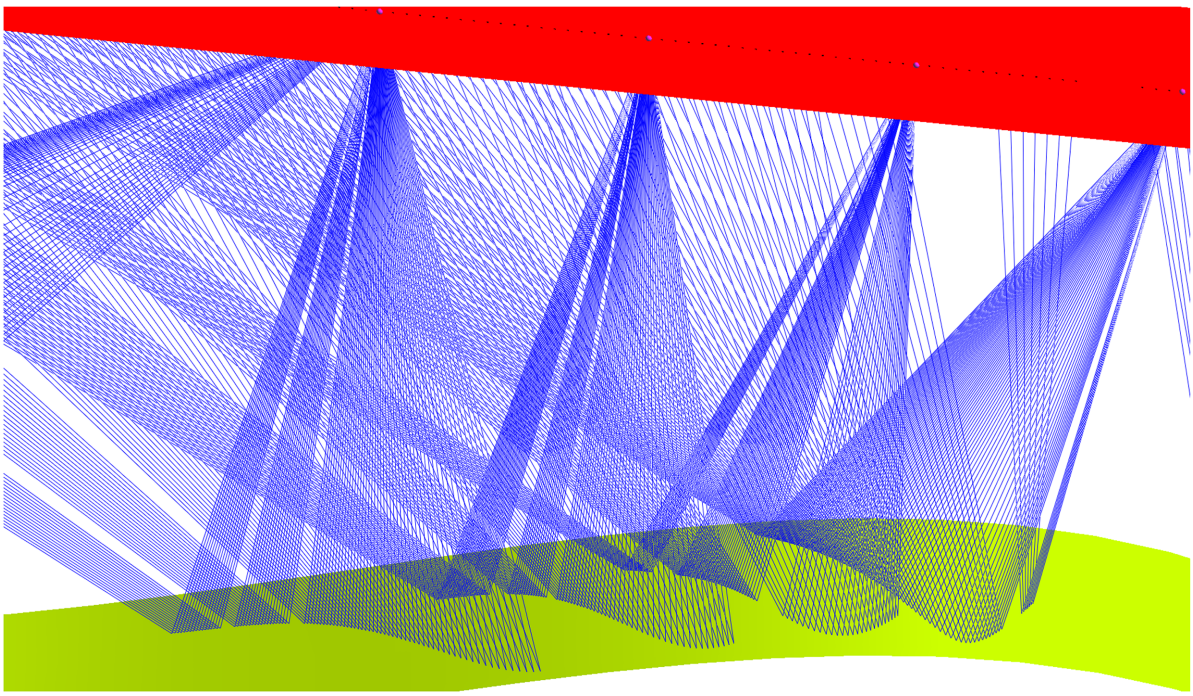

Figure 3 Detailed view of two-point rays of the reflected S2S1 wave for shots 80, 100, 120 and 140. Note the curved paths of reflections at the interface.

(2.5D velocity model, see Figs 1 and 2). The triclinic asymmetry causes that the two-point rays do not stay in the vertical planes corresponding to the individual profiles (see Fig. 3).

Slowness and ray-velocity surfaces

We generate and display the slowness and ray-velocity surfaces for the triclinic anisotropy given by matrix (1) to show complexity of the S1, S2 and converted waves. The slowness surface (phase-slowness surface, index surface) at spatial point x^m is composed of three sheets corresponding to the three eigenvalues of the Christoffel matrix (Klimeš, 2002). Analogously, the ray-velocity surface (group-velocity surface, Fresnel wave surface) at spatial point x^m is composed of three sheets corresponding to the three eigenvalues of the Christoffel matrix.

Although slowness and ray-velocity surfaces of the P waves are convex and smooth (see Figs 4 and 6), the surfaces of the ray-theory S1 and S2 waves are much more complex (see Figs 5 and 7–11). We display ray-velocity surfaces in solid wireframe mode to see the anomalies with more contrast. The detailed study of S1 and S2 surfaces shows many common, singular points. We highlighted several triplications (**T**), concave parts of point singularities (**S**) and diffraction (convex) parts of point singularities (**D**) on slowness surfaces. Note the different shapes and slightly different positions of these caustics for slowness compared to ray-velocity surfaces (see Figs 8–11). Surfaces are plotted in the same three-dimensional view and the different positions of caustics are caused by different directions of slowness and ray-velocity vectors. Some parts of slowness and ray-velocity surfaces are concaved and for ray-velocity surfaces even intersect. All these anomalies cause ray-theory calculation problems in some directions.

The velocity model with triclinic anisotropy in the upper layer is homogeneous. Thus we can plot ray-velocity vectors at the source and receivers together with ray-velocity surfaces for individual common-shot gathers to see which parts of ray-velocity surfaces are hitted by starting and end points of rays. Detailed study of all common-shot gathers and all elementary waves is out of the scope of this paper, where we present ray-velocity vectors and ray diagrams only for two common-shot gathers and reflected wave S2S2. Figure 12 displays the ray diagram and the part of ray-velocity surface with vectors for shot 20 ($x_1 = 3.475$ km) that is simple compared to Fig. 13 for shot 80 ($x_1 = 4.975$ km), where we observe triplications. Figures 14 and 15 show synthetic seismograms and travel times for the same common-shots 20 and 80.

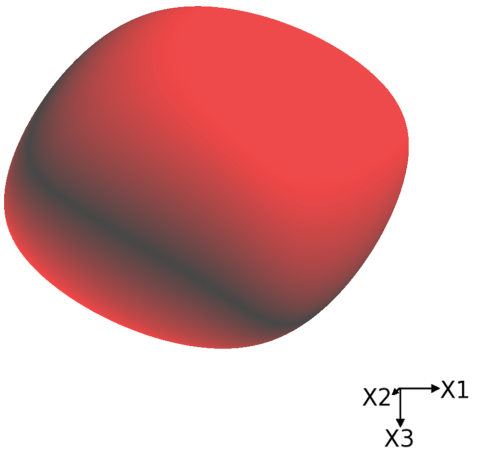

Figure 4 The P wave slowness surface for the triclinic anisotropy.

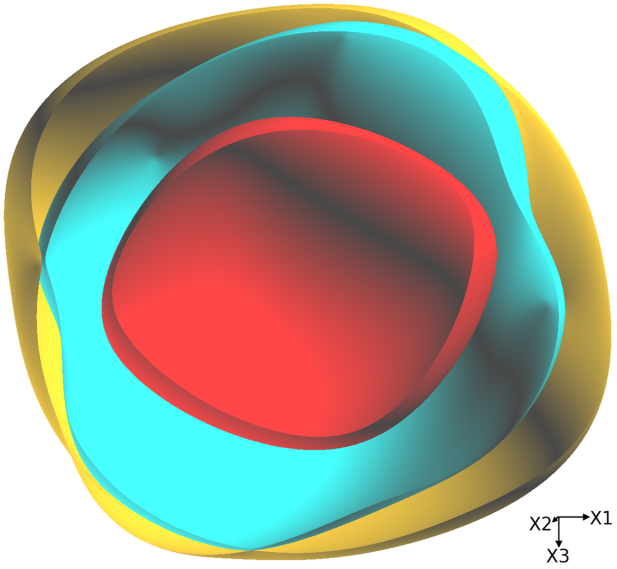

Figure 5 The sliced P, S1 and S2 wave slowness surfaces for the triclinic anisotropy.

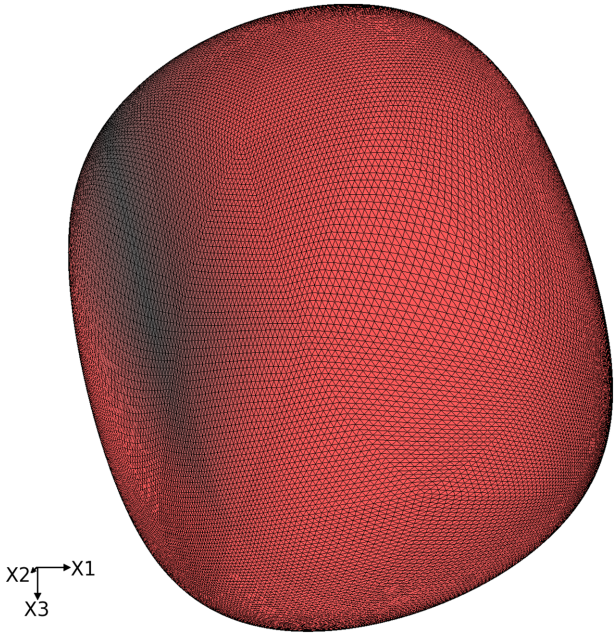

Figure 6 The P wave ray-velocity surface for the triclinic anisotropy.

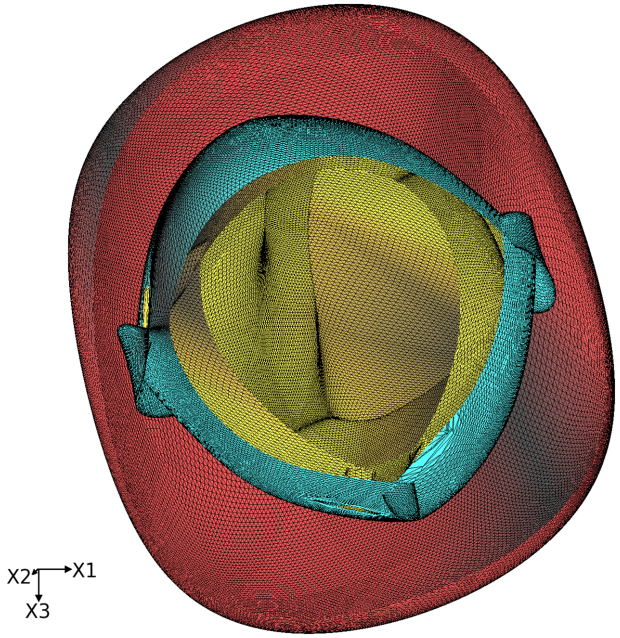

Figure 7 The sliced P, S1 and S2 wave ray-velocity surfaces for the triclinic anisotropy.

Synthetic seismograms

We use an explosive source for calculation of ray-theory synthetic seismograms. The source-time function is a Gabor wavelet, $\exp[-(2\pi f/\gamma)^2 2t^2]\cos(2\pi ft)$, with the dominant frequency $f = 25$ Hz and $\gamma = 1$.

Figures 14 and 15 show radial, transversal and vertical components of the seismograms for nine elementary reflected and converted waves for two selected shot-receiver configurations: PP, PS1, PS2, S1P, S2P, S1S1, S2S1, S1S2 and S2S2 waves. Notation is simple, the first letter denotes the elementary wave type from the source to the reflection point and the second letter denotes the elementary wave type from the reflection point to the receiver. P is for P waves, S1 and S2 are for ray-theoretical S waves. We display seismograms for common-shots 20 and 80 ($x_1 = 3.475$ km and 4.975 km).

The relatively strong triclinic anisotropy causes the generation of strong S1, S2 and converted waves even for an

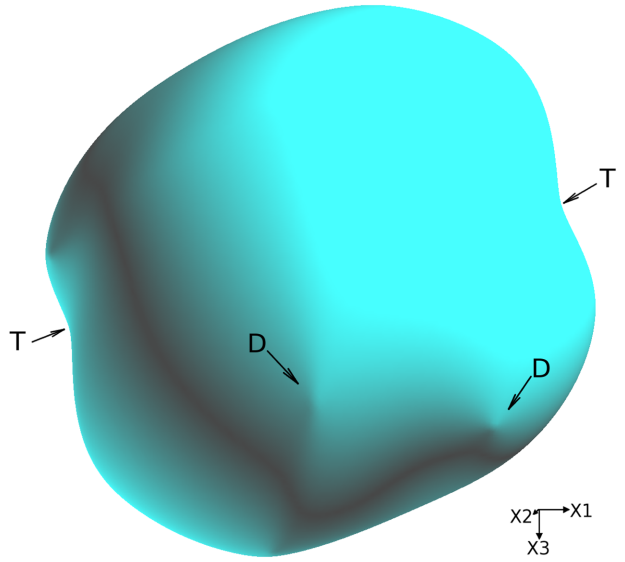

Figure 8 The S1 wave slowness surface for the triclinic anisotropy. **T** denotes the triplication and **D** diffraction (convex) part of the point singularity.

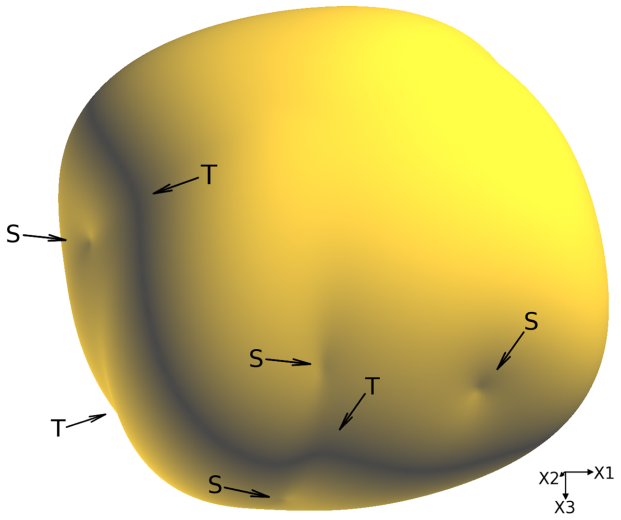

Figure 9 The S2 wave slowness surface for the triclinic anisotropy. **T** denotes the triplication and **S** concave part of the point singularity.

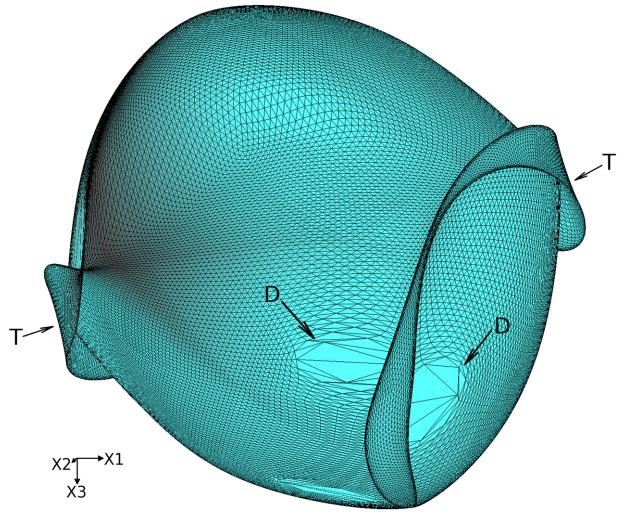

Figure 10 The S1 wave ray-velocity surface for the triclinic anisotropy. **T** denotes the triplication and **D** the point singularity.

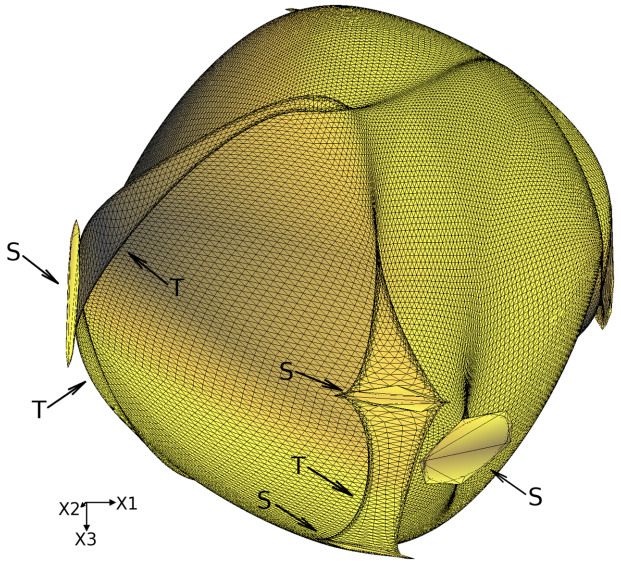

Figure 11 The S2 wave ray-velocity surface for the triclinic anisotropy. **T** denotes the triplication and **S** the point singularity.

explosive source (see Figs 14 and 15). To assess the ratio of amplitudes, we plot seismograms of all waves for each shot with the same scale. Waves with relatively small amplitudes are poorly visible, thus we added travel times.

For the P, S1, S2 and converted waves, we observe receivers experiencing a change in the sign of the reflection coefficient around a region of the nearly vanishing reflection coefficient (Fig. 14). This is caused by the fact that the value of the corresponding elementary wave velocity in the isotropic bottom layer is between the values of the horizontal (axis x_1) and vertical (axis x_3) wave velocities in anisotropic upper layer (for details, please refer to Bucha, 2017). On the other hand, for S1, S2 and converted waves, we observe seismograms with enormous amplitudes for some shot-receiver configurations, caused probably by singularities. Triplications for the S2S2 wave, highlighted in Fig. 13, are visible in Fig. 15 near the time 2.5 seconds.

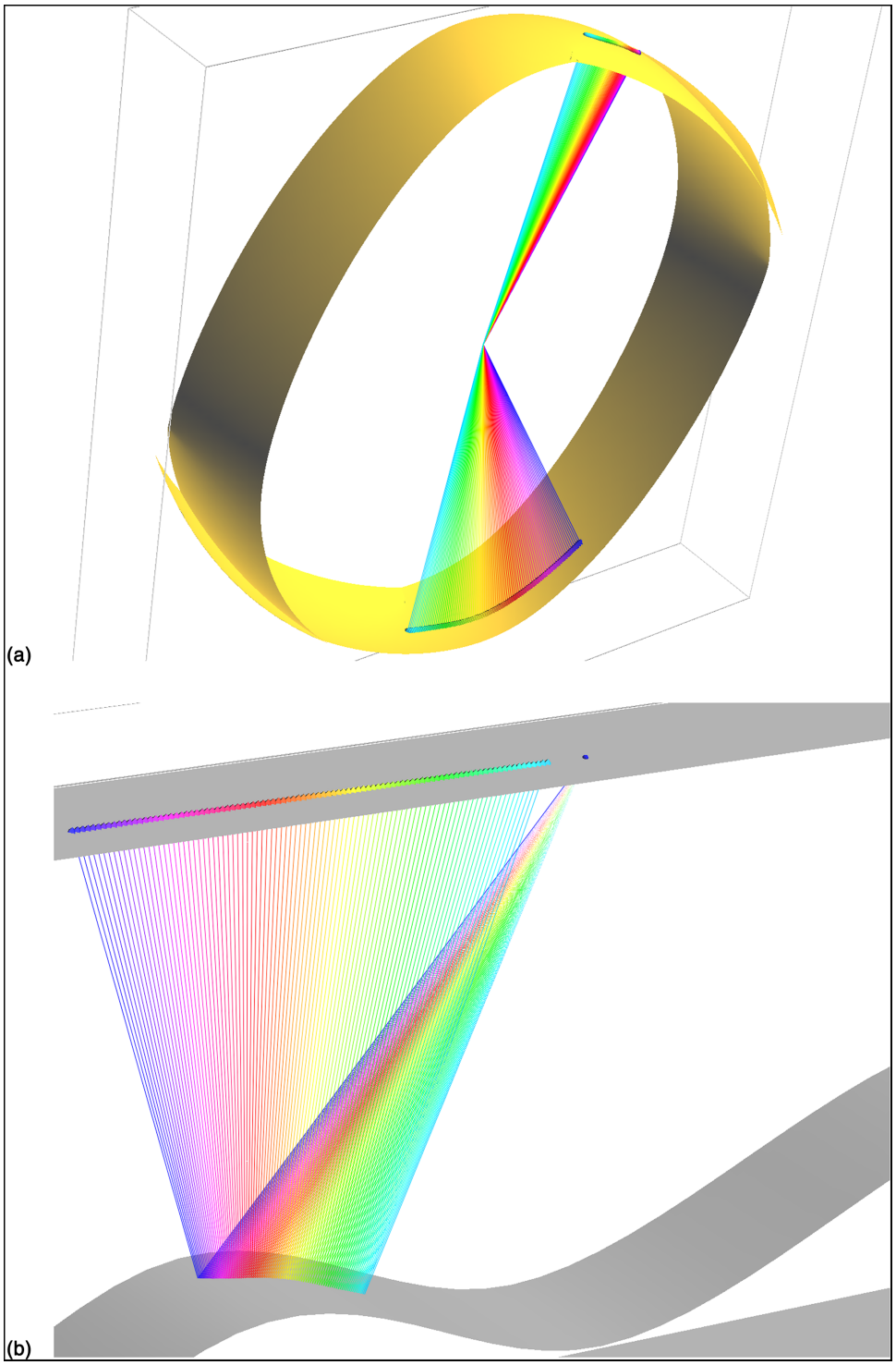

Figure 12 Two displays for the single common-shot gather corresponding to shot 20 ($x_1 = 3.475$ km): (a) Sliced S2 wave ray-velocity surface with ray-velocity vectors at the source (small spheres at the top of the surface) and ray-velocity vectors at the receivers (small diamonds at the bottom of the surface) of the reflected S2S2 wave. Colours of points and lines correspond to the index value of the receivers. (b) Sliced velocity model with two-point rays of the reflected S2S2 wave. Colours of rays and receivers correspond to the index value of the receivers.

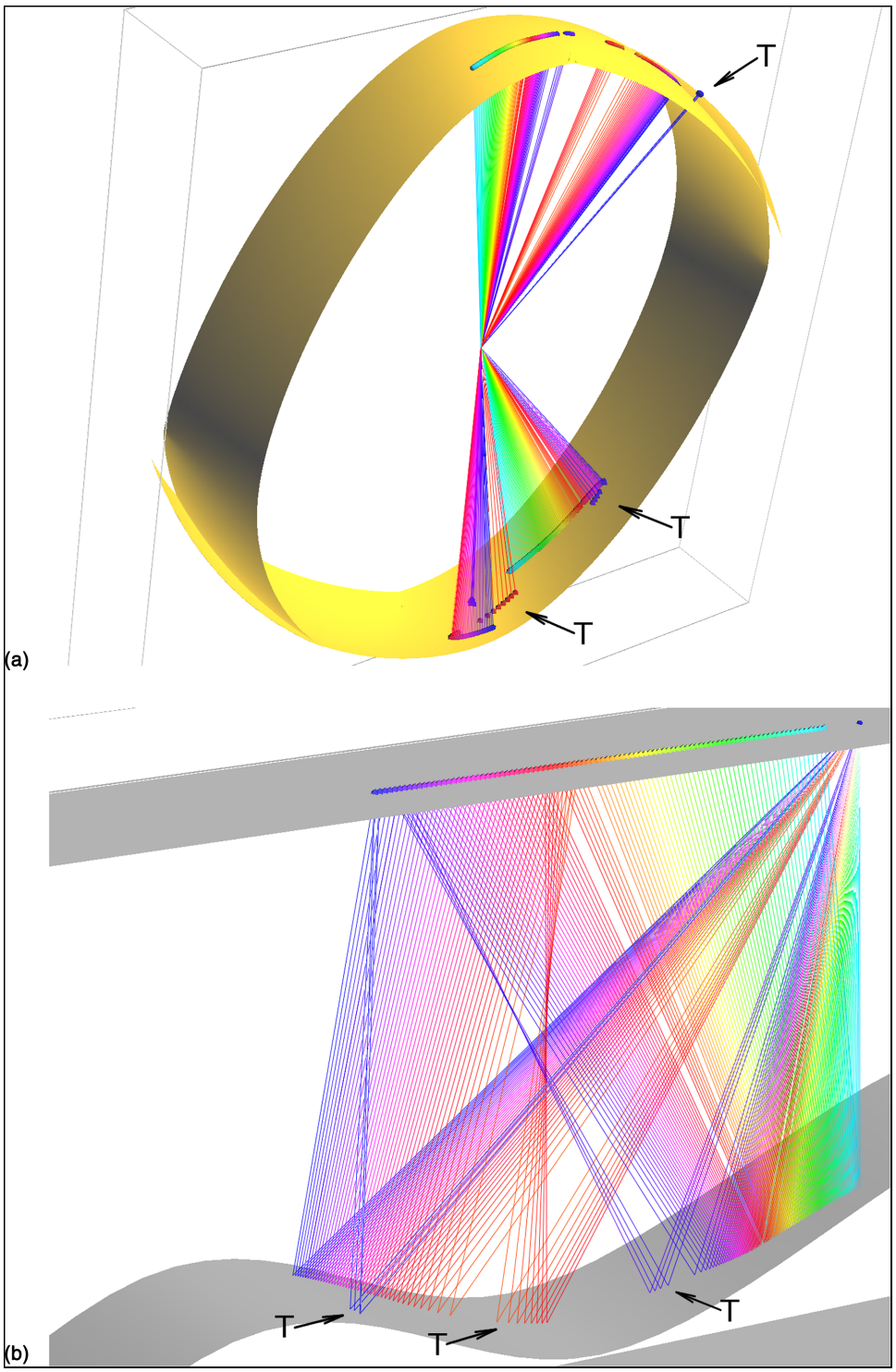

Figure 13 Two displays for the single common-shot gather corresponding to shot 80 ($x_1 = 4.975$ km): (a) Sliced S2 wave ray-velocity surface with ray-velocity vectors at the source (small spheres at the top of the surface) and ray-velocity vectors at the receivers (small diamonds at the bottom of the surface) of the reflected S2S2 wave. Colours of points and lines correspond to the index value of the receivers. (b) Sliced velocity model with two-point rays of the reflected S2S2 wave. Colours of rays and receivers correspond to the index value of the receivers. **T** denotes the triplication.

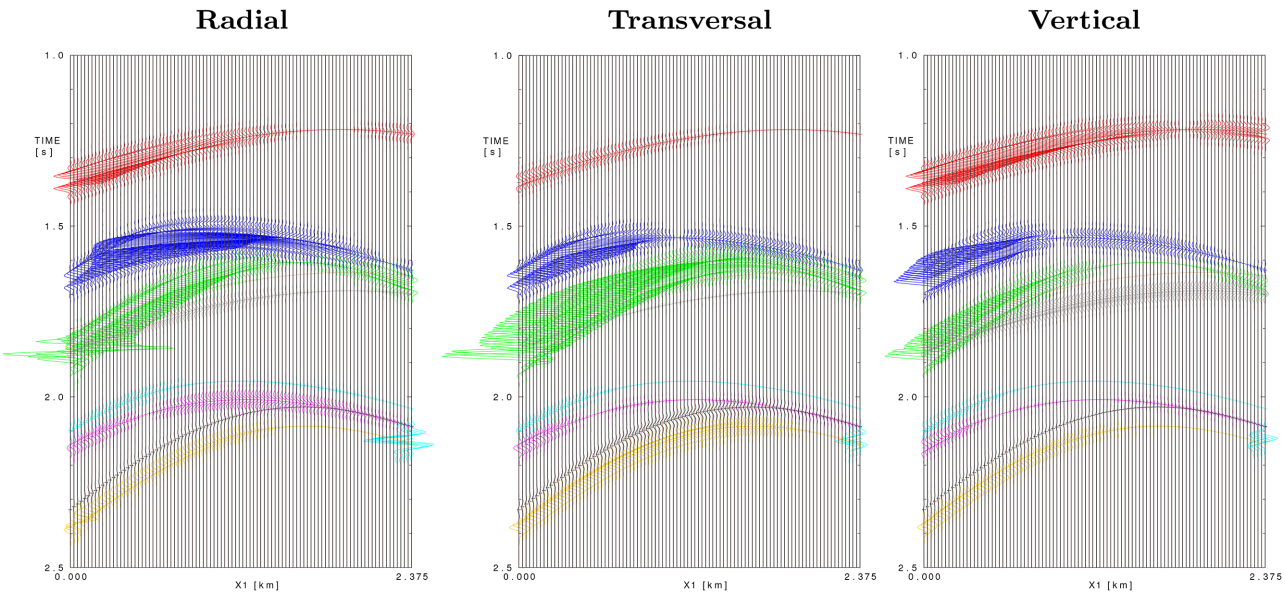

Figure 14 Radial (X1), transversal (X2) and vertical (X3) components of synthetic seismograms and travel times of the reflected P, S1, S2 and converted waves for the single common-shot gather at line $x_2 = 5$ km corresponding to shot 20 ($x_1 = 3.475$ km). The nine elementary waves, ordered approximately according to their travel time from the smallest, PP wave, PS1 wave, PS2 wave, S1P wave, S2P wave, S1S1 wave, S2S1 wave, **S1S2** wave and S2S2 wave. All seismograms are scaled the same.

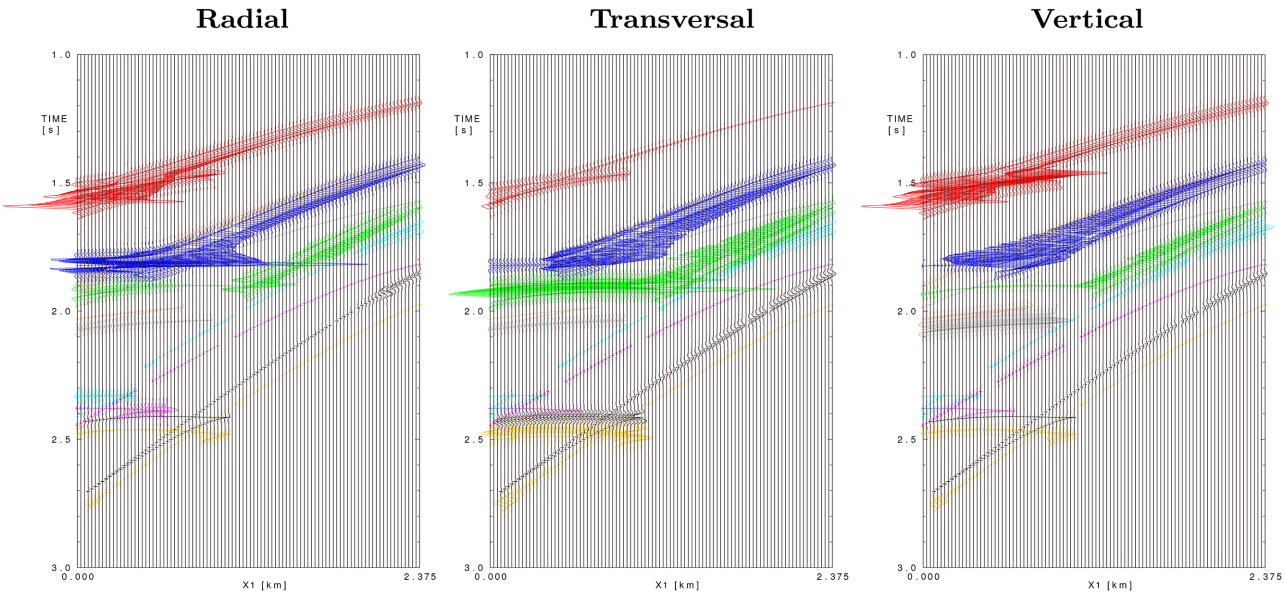

Figure 15 Radial (X1), transversal (X2) and vertical (X3) components of synthetic seismograms and travel times of the reflected P, S1, S2 and converted waves for the single common-shot gather at line $x_2 = 5$ km corresponding to shot 80 ($x_1 = 4.975$ km). The nine elementary waves, ordered approximately according to their travel time from the smallest, PP wave, PS1 wave, PS2 wave, S1P wave, S2P wave, S1S1 wave, S2S1 wave, **S1S2** wave and S2S2 wave. All seismograms are scaled the same.

KIRCHHOFF PRE-STACK DEPTH SCALAR MIGRATION

For scalar migration, we migrate a single seismogram component using the scalar ray-theory amplitude instead of the vectorial ray-theory amplitude. We use the MODEL, CRT, FORMS and DATA software packages for the three-dimensional Kirchhoff pre-stack depth scalar migration (Červený *et al.*, 1988; Bulant, 1996; Bucha and Bulant, 2019).

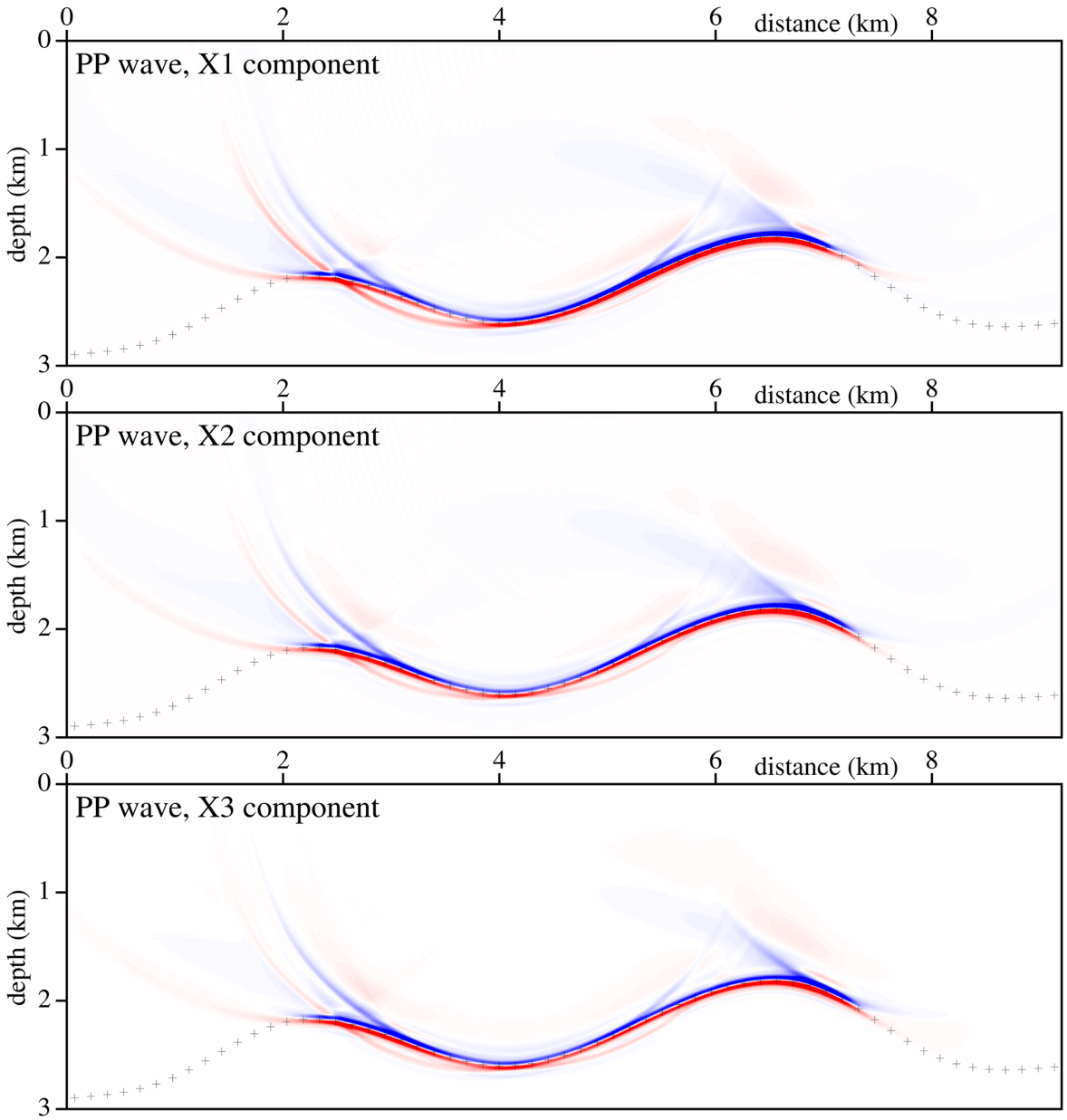

Figure 16 Stacked migrated sections calculated in the triclinic velocity model without interface. Radial (X1), transversal (X2) and vertical (X3) components of PP reflected wave are used. 81 × 240 common-shot pre-stack depth migrated sections, corresponding to 81 profile lines and 240 sources along each profile line, have been stacked. The crosses denote the interface in the velocity model used to compute the recorded wave field.

We migrate separately individual components of individual waves. The ray-based migration of each component separately means that we migrate only a specific portion of the wave field corresponding to a specific portion of the migrated interface.

The migration algorithm consists of two-parametric controlled initial-value ray tracing (Bulant, 1999) from the individual surface points, calculating grid values of travel times and amplitudes by interpolation within ray cells (Bulant and Klimeš, 1999). The paraxial approximation of travel times from the carefully selected nearest ray (Waheed *et al.*, 2013) is an alternative approach to calculating travel times for migration in inhomogeneous media to avoid interpolation.

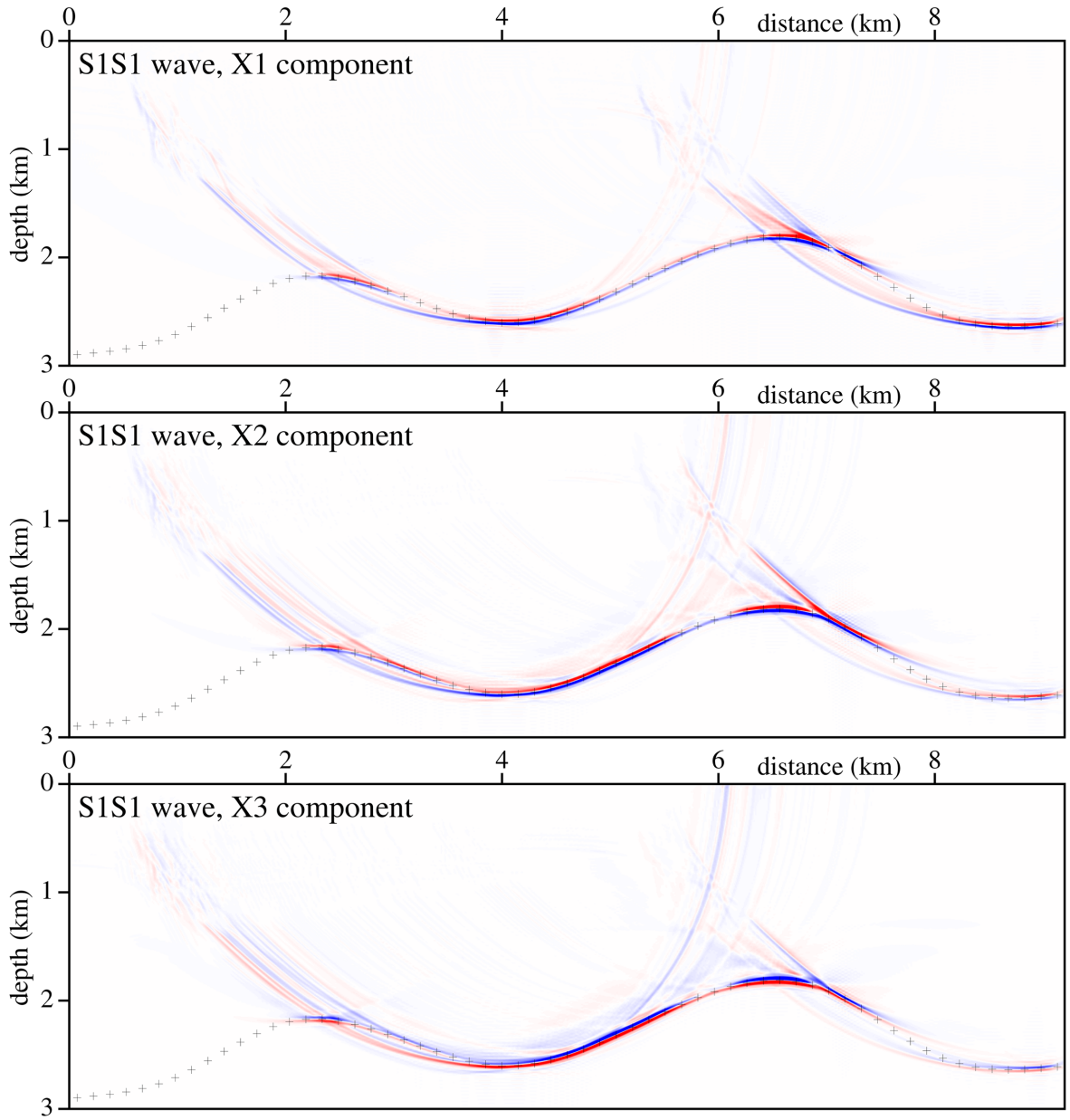

Figure 17 Stacked migrated sections calculated in the triclinic velocity model without interface. Radial (X1), transversal (X2) and vertical (X3) components of S1S1 reflected wave are used. 81 × 240 common-shot pre-stack depth migrated sections, corresponding to 81 profile lines and 240 sources along each profile line, have been stacked. The crosses denote the interface in the velocity model used to compute the recorded wave field.

Then we perform the common-shot migration and stack the migrated images. The shot-receiver configuration consists of 81 parallel profile lines at intervals of 0.025 km (see Fig. 2). The first profile line is situated at horizontal coordinate $x_2 = 4$ km and the last profile line is situated at horizontal coordinate $x_2 = 6$ km. For migration, we use the single-layer velocity model (without the interface) with the same triclinic anisotropy as in the upper layer of the velocity model used to calculate the recorded wave field given by matrix (1).

In our tests, we calculate only one vertical image section corresponding to the central profile line ($x_2 = 5$ km, see Fig. 2). Although it is only a two-dimensional profile line, such an image represents one vertical section of full 3D migrated volume. We form the image by computing and summing the

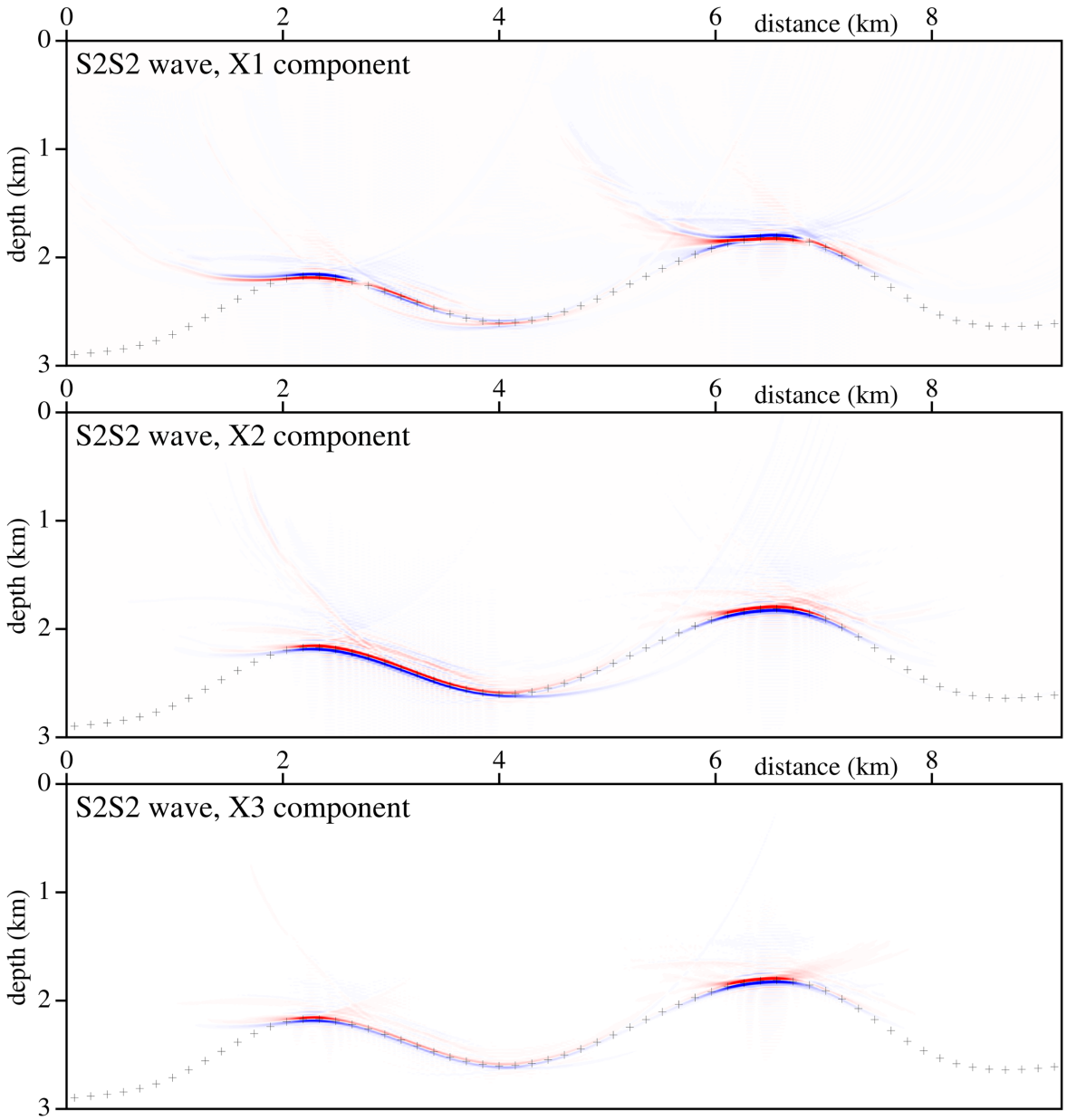

Figure 18 Stacked migrated sections calculated in the triclinic velocity model without interface. Radial (X1), transversal (X2) and vertical (X3) components of S2S2 reflected wave are used. 81 × 240 common-shot pre-stack depth migrated sections, corresponding to 81 profile lines and 240 sources along each profile line, have been stacked. The crosses denote the interface in the velocity model used to compute the recorded wave field.

corresponding contributions (images) from all 81 parallel source–receiver lines. While summing the contributions, the constructive interference focuses the migrated interface and the destructive interference reduces undesirable migration artefacts (non-specular reflections). We also use cosine taper to clear artefacts, but some of them, especially residual semi-circular smiles, remain.

DISCUSSION

During calculations, we encounter problems with anomalous amplitudes of the Green function for S1S1, S2S2, S1S2, S2S1, PS1 and PS2 waves caused by singularities for some common-shot gathers. These anomalies yield additional migration artefacts (noise). We solved the problem by limiting the

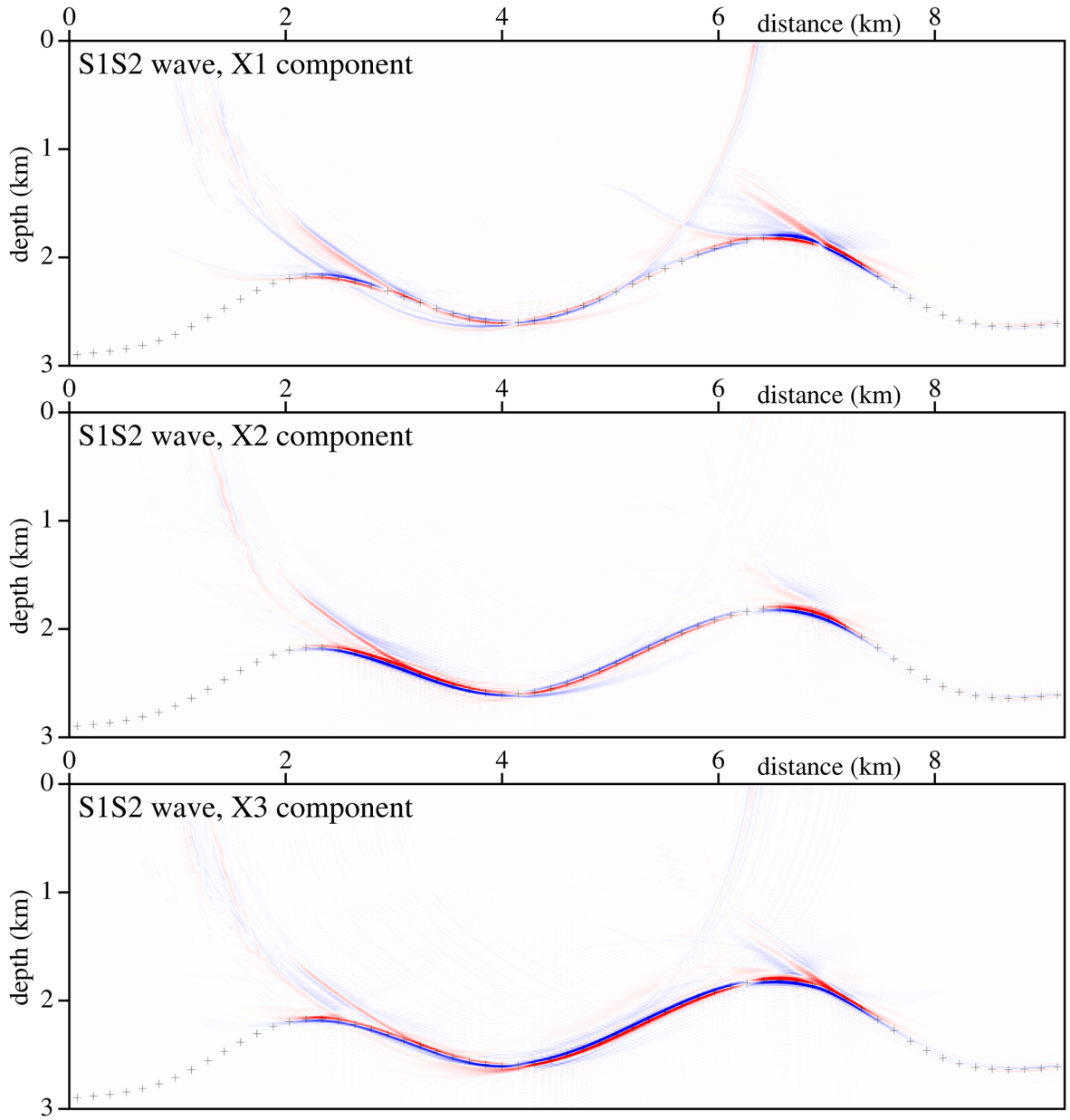

Figure 19 Stacked migrated sections calculated in the triclinic velocity model without interface. Radial (X1), transversal (X2) and vertical (X3) components of S1S2 reflected wave are used. 81 × 240 common-shot pre-stack depth migrated sections, corresponding to 81 profile lines and 240 sources along each profile line, have been stacked. The crosses denote the interface in the velocity model used to compute the recorded wave field.

maximum value of the scalar ray-theory amplitude of the Green's function.

Figure 16 shows stacked migrated sections calculated separately for radial, transversal and vertical components of reflected PP wave. The migrated interface is clear and coincides nearly perfectly with the interface in the velocity model used to compute the recorded wave field.

Analogously, Figs 17–20 show stacked migrated sections calculated separately for three components of the reflected ray-theory S1S1, S2S2, S1S2 and S2S1 elementary waves. The results are worse than for the PP wave. Some parts of migrated interface are poorly imaged. We see differences among individual components for separate elementary waves.

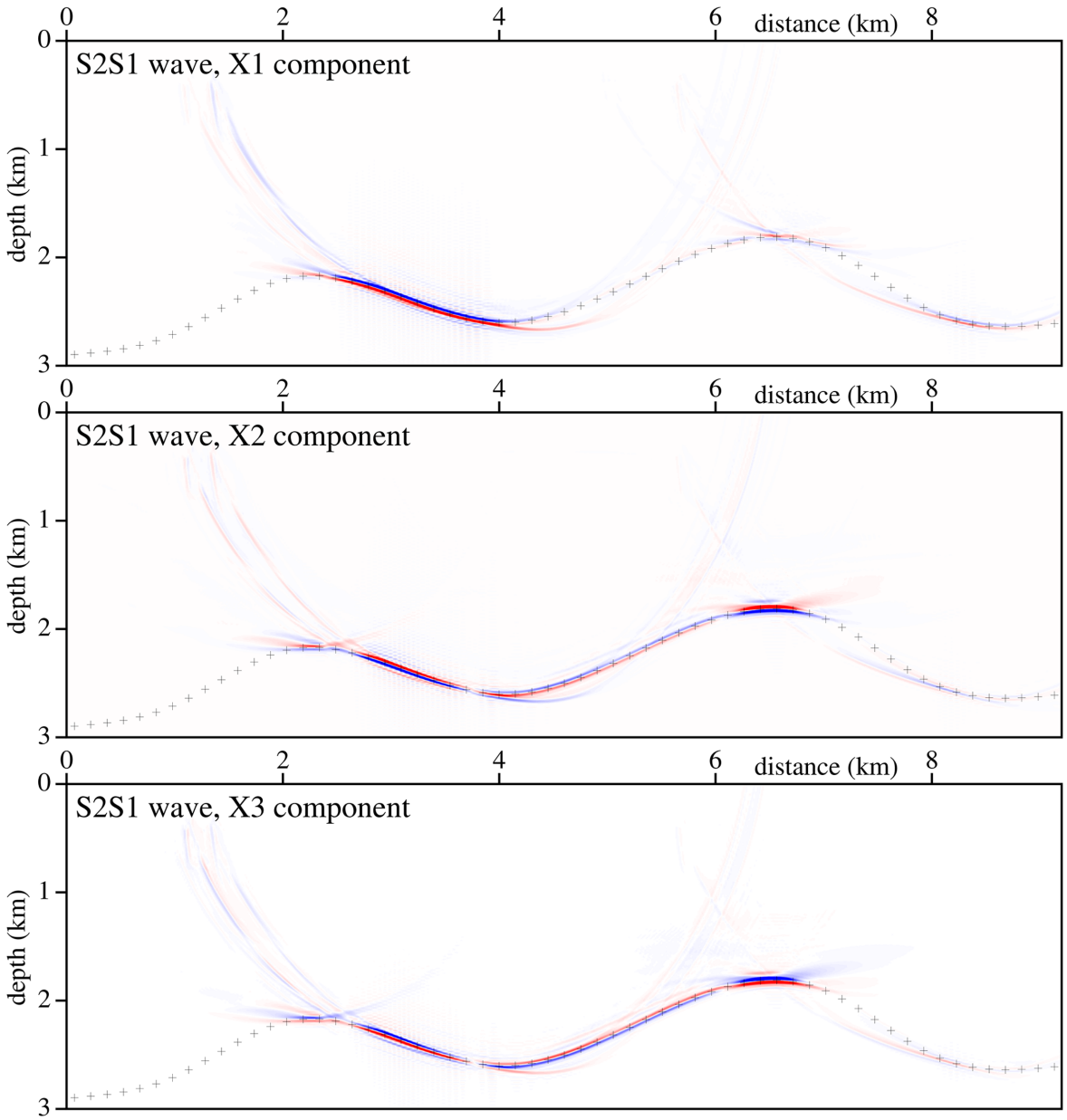

Figure 20 Stacked migrated sections calculated in the triclinic velocity model without interface. Radial (X1), transversal (X2) and vertical (X3) components of S2S1 reflected wave are used. 81 × 240 common-shot pre-stack depth migrated sections, corresponding to 81 profile lines and 240 sources along each profile line, have been stacked. The crosses denote the interface in the velocity model used to compute the recorded wave field.

Note several combinations of reverse (flipped polarity) amplitudes in migrated sections for S1S1, S2S2, S1S2 and S2S1 elementary waves. For example, radial (X1) component has reverse amplitudes than transversal (X2) and vertical (X3) components of S2S2 wave (see Fig. 18). Vertical components (X3) for S1S1 and S1S2 waves have reverse amplitudes with respect to S2S2 and S2S1 waves (see Figs 17–20). Moreover, some parts of the same migrated interface have alternating amplitudes (see Fig. 19). The summation of all sections thus might diminish the result.

Migrated interfaces for the radial (X1) component of PS1 converted wave (see Fig. 21) and for transversal (X2) component of PS2 converted wave (see Fig. 22) are clear and coincide nearly perfectly with the interface in the velocity model used

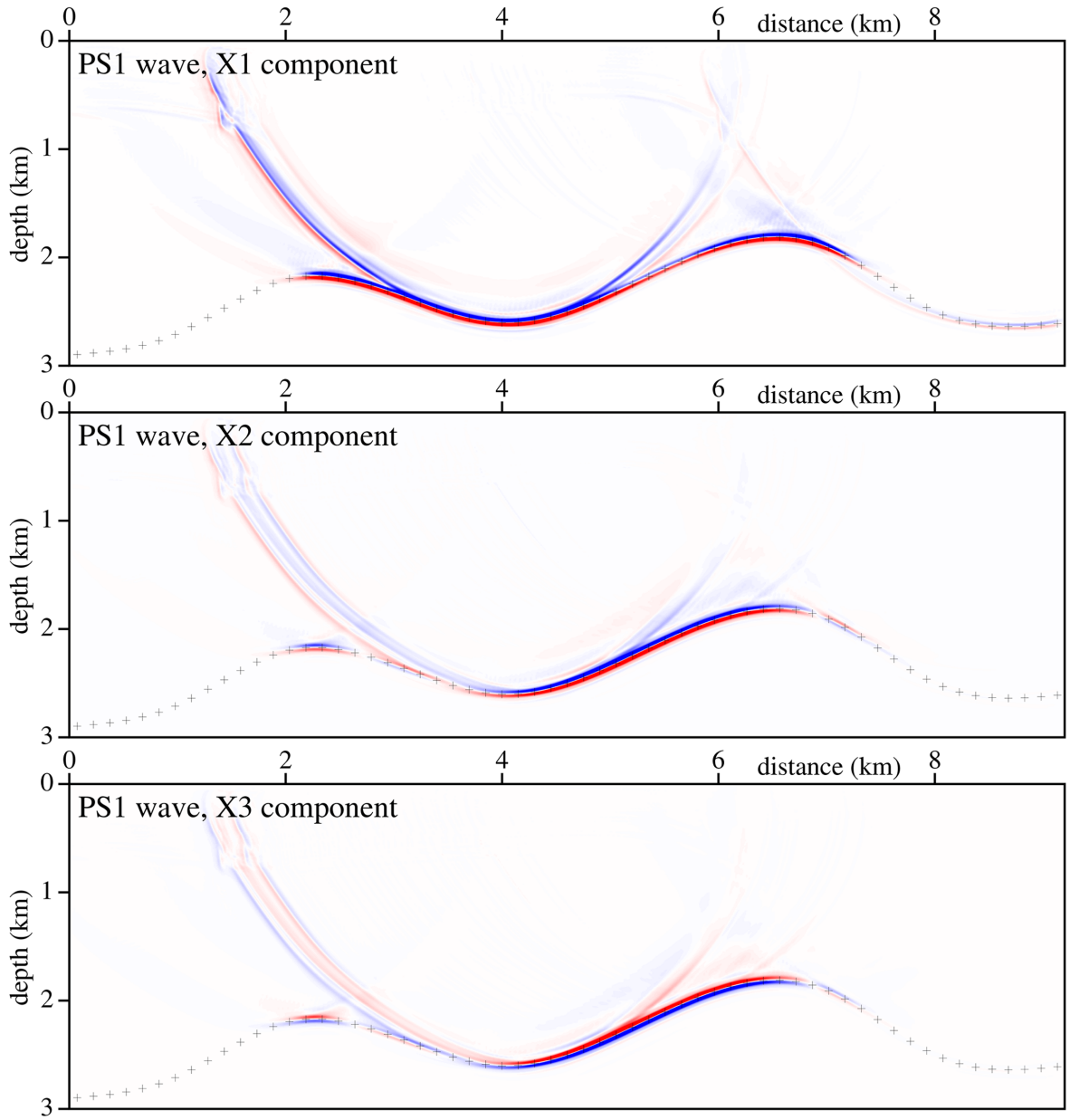

Figure 21 Stacked migrated sections calculated in the triclinic velocity model without interface. Radial (X1), transversal (X2) and vertical (X3) components of PS1 converted wave are used. 81 × 240 common-shot pre-stack depth migrated sections, corresponding to 81 profile lines and 240 sources along each profile line, have been stacked. The crosses denote the interface in the velocity model used to compute the recorded wave field.

to compute the recorded wave field. All other migrated interfaces for other components of converted PS1, PS2, S1P and S2P elementary waves have some parts of the migrated sections poorly imaged (see Figs 21–24). Similarly to reflected S1 and S2 waves, note several combinations of reverse migration amplitudes. Several migrated sections contain strong migration artefacts, smiles, that will be subject of further study.

The poorly imaged parts of interface are probably caused by the complex ray-theory synthetic wave field. Amplitudes of the wave field for some common shot gathers are influenced by the change of the sign of the reflection coefficient around a region of the nearly vanishing reflection coefficient. This is caused by the fact that the value of the corresponding elementary wave velocity in isotropic bottom layer is between the

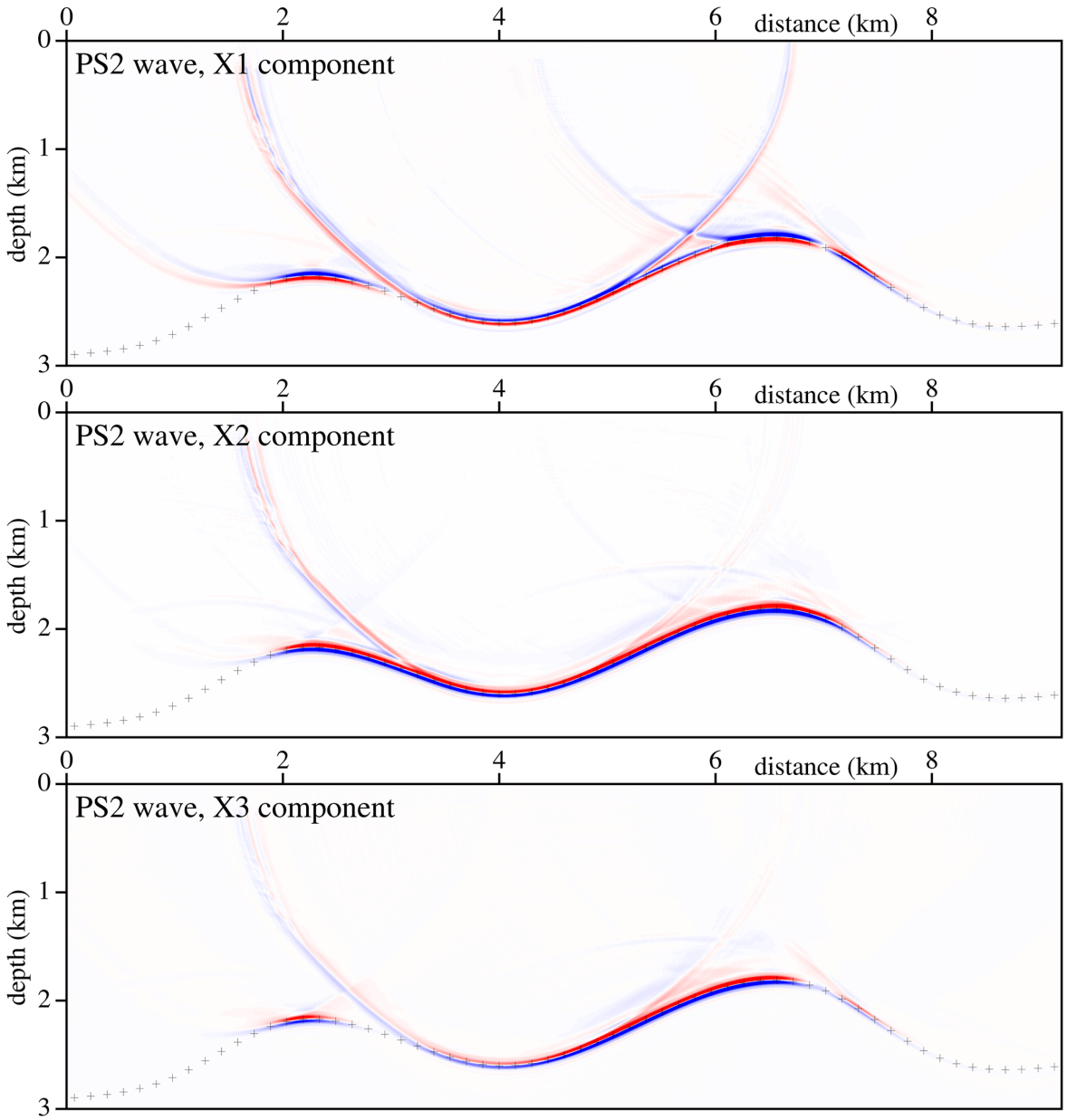

Figure 22 Stacked migrated sections calculated in the triclinic velocity model without interface. Radial (X1), transversal (X2) and vertical (X3) components of PS2 converted wave are used. 81 × 240 common-shot pre-stack depth migrated sections, corresponding to 81 profile lines and 240 sources along each profile line, have been stacked. The crosses denote the interface in the velocity model used to compute the recorded wave field.

values of the horizontal (axis x_1) and vertical (axis x_3) wave velocities in anisotropic upper layer. On the other side, we observe some short parts of the wave field with enormous amplitudes for some shot-receiver configurations, caused probably by singularities. Anomalies of the ray-velocity S1 and S2 surfaces cause ray-theory calculation problems in some directions (missing rays). Another reason of poorly imaged interface is probably the curvature of the interface, which along with the waves radiation patterns from the source and the reflector may cause limited illumination in certain regions of the reflector.

We currently do not have specific explanations for badly imaged parts of the interface. This will require an analysis of the reflection coefficient for the interface, which is a func-

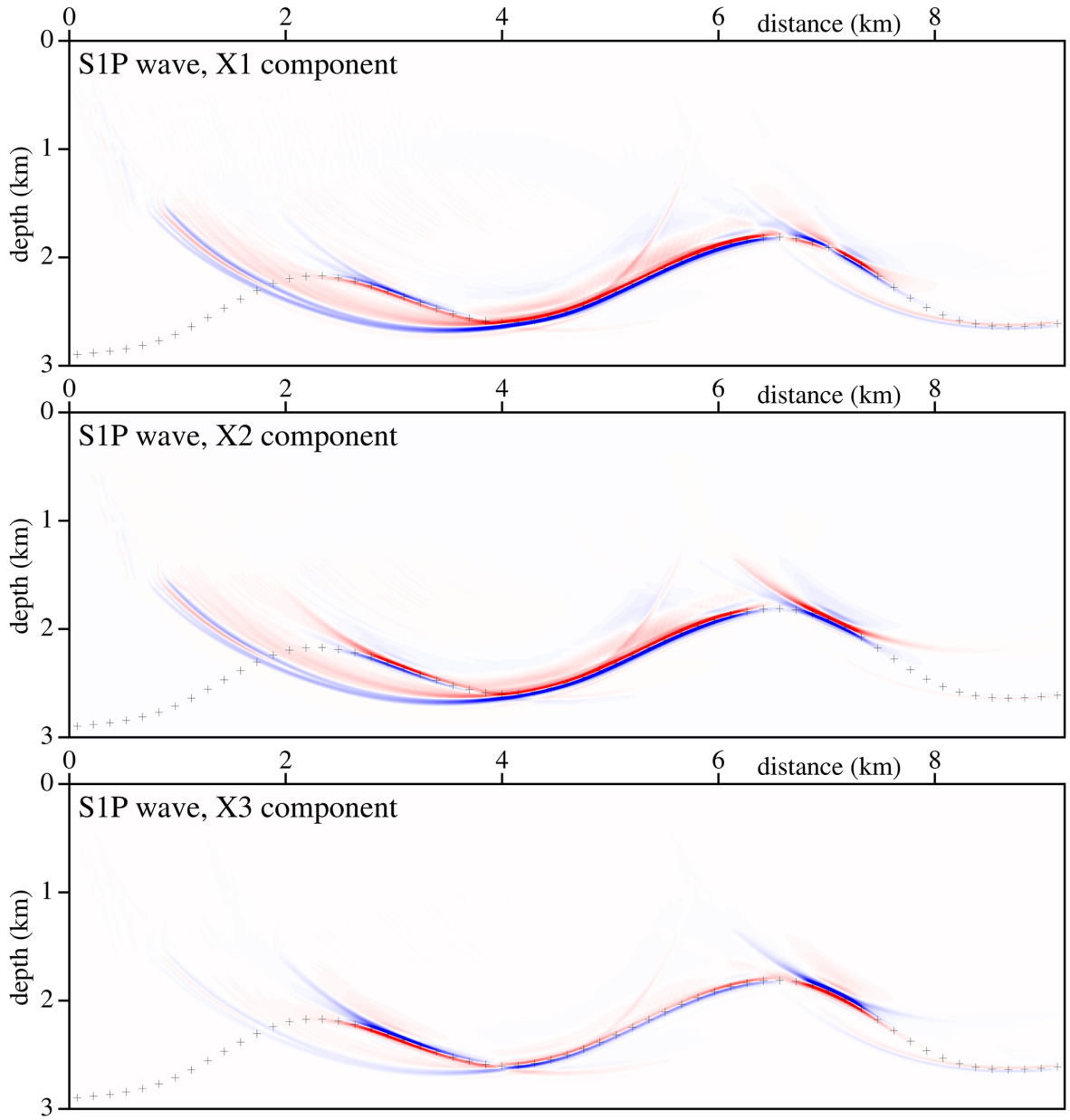

Figure 23 Stacked migrated sections calculated in the triclinic velocity model without interface. Radial (X1), transversal (X2) and vertical (X3) components of S1P converted wave are used. 81 × 240 common-shot pre-stack depth migrated sections, corresponding to 81 profile lines and 240 sources along each profile line, have been stacked. The crosses denote the interface in the velocity model used to compute the recorded wave field.

tion of two group velocity vectors that are hard to analyse or display.

The presented ray-based migration algorithm was tested with separate components of individual elementary waves. Nevertheless, the real complete wave field is difficult to separate into modes. We tested our scalar imaging algorithm with the synthetic complete wave field in simple inhomogeneous weakly anisotropic velocity models (Bucha, 2019). The complete wave field was calculated by the Fourier pseudo-spectral method (Tessmer, 1995). We have imaged the vertical component of the PP reflected wave, radial and transversal components of PS1 and PS2 converted waves. In spite of the complex recorded wave fields, the imaged interfaces are, in all stacked migrated sections, relatively good. The destructive interference

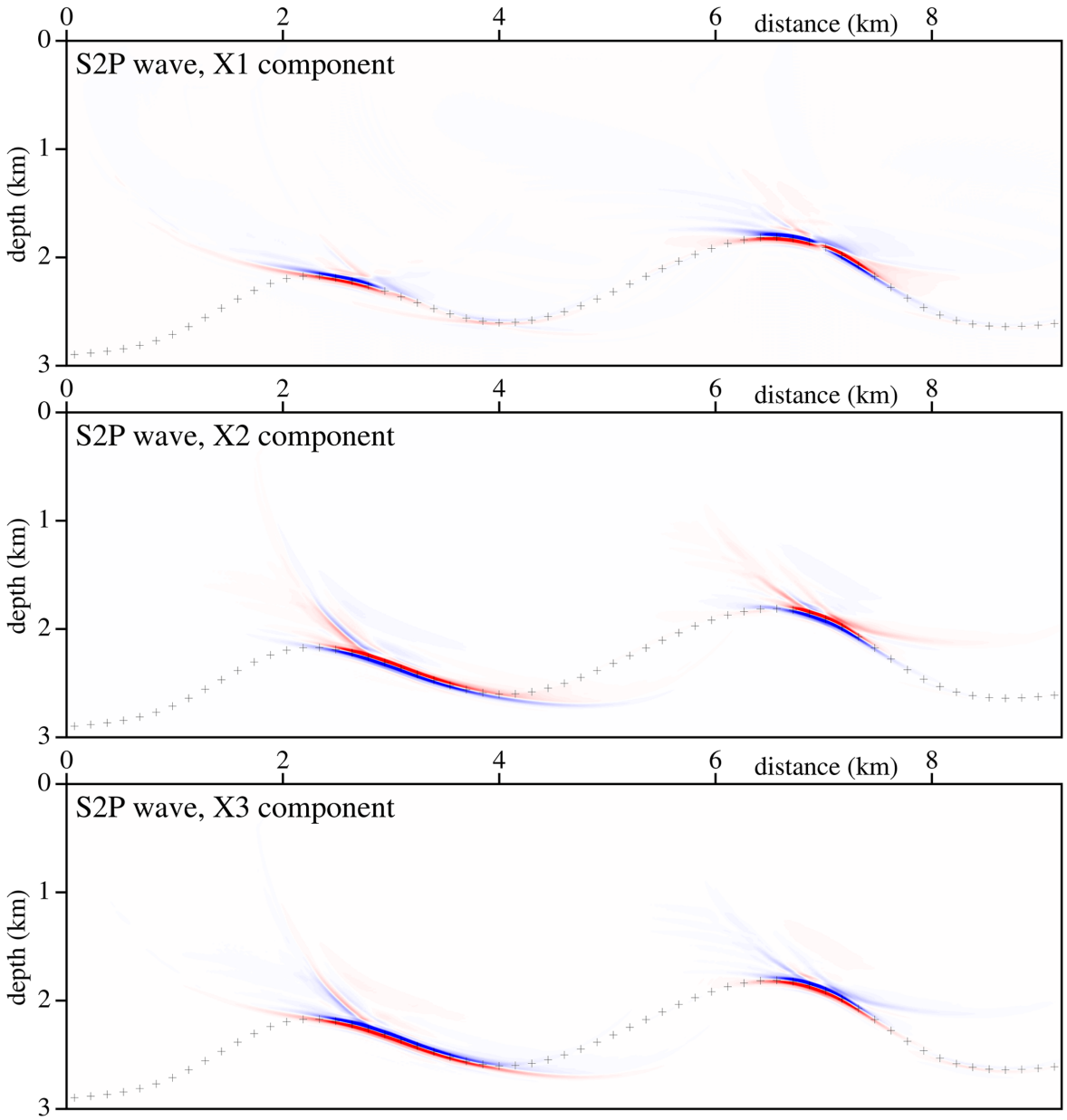

Figure 24 Stacked migrated sections calculated in the triclinic velocity model without interface. Radial (X1), transversal (X2) and vertical (X3) components of S2P converted wave are used. 81 × 240 common-shot pre-stack depth migrated sections, corresponding to 81 profile lines and 240 sources along each profile line, have been stacked. The crosses denote the interface in the velocity model used to compute the recorded wave field.

reduces and smudges the undesirable migration artefacts with exception to spurious interface images close to the correct ones (for converted waves).

It is well known that ray-method is problematic at singularity points and triplications. Despite the complex triclinic anisotropy, all calculations both for recorded wave field and for migration were accomplished and that demonstrates computational stability of the used codes. For inhomogeneous media, we can use travel time compression (e.g. Alkhalifah, 2011), which will also help smooth the traveltime fields to reduce artefacts.

Other alternatives for imaging calculations are Gaussian beams or packet methods. We applied our codes to two-dimensional acoustic imaging of the Marmousi model and

we got nearly the same or better migrated sections using ray-method imaging compared to the Gaussian packet approach. Moreover the computation time was multiple times less for ray-method imaging.

CONCLUSIONS

We generated three-component synthetic seismograms of P, S1, S2 and converted waves using ray theory in a simple two-layer velocity model composed of two homogeneous layers with relatively strong triclinic anisotropy in the upper layer. We then applied the three-dimensional ray-based Kirchhoff pre-stack depth scalar migration to the homogeneous single-layer velocity model with the same triclinic anisotropy. We migrated individual components of individual elementary waves separately.

The migrated interface is clear and coincides nearly perfectly with the interface in the velocity model used to compute the recorded wave field for:

1. radial, transversal and vertical components of reflected PP wave,
2. radial component of PS1 converted wave,
3. transversal component of PS2 converted wave.

The quality of migrated sections for other elementary waves fluctuates. Some parts of the migrated interface are imaged clearly, some poorly. Detailed explanation of poorly imaged parts of interface and change to vector migration instead of scalar approach will be a subject of further study.

ACKNOWLEDGEMENTS

The author thanks Luděk Klimeš and Ivan Pšenčík for their help throughout the work on this paper. The author would also like to thank two reviewers and associate editor for many helpful recommendations to improve the manuscript.

The research has been supported by the Czech Science Foundation under Contract 20-06887S, and by the members of the consortium 'Seismic Waves in Complex 3-D Structures' (see 'http://sw3d.cz').

DATA AVAILABILITY STATEMENT

The data that support the findings of this study are available from the corresponding author upon reasonable request.

ORCID

Václav Bucha https://orcid.org/0000-0002-3023-8541

REFERENCES

Alkhalifah, T. (2006) Kirchhoff time migration for transversely isotropic media: an application to Trinidad data. *Geophysics*, 71, S29.

Alkhalifah, T. (2011) Efficient traveltime compression for 3-D prestack Kirchhoff migration. *Geophysical Prospecting*, 59, 1–9.

Alkhalifah, T. and Larner, K. (1994) Migration error in transversely isotropic media. *Geophysics*, 59, 1405–1418.

Bucha, V. (2012) Kirchhoff prestack depth migration in 3-D simple models: comparison of triclinic anisotropy with simpler anisotropies. *Studia Geophysica et Geodaetica*, 56, 533–552.

Bucha, V. (2013) Kirchhoff prestack depth migration in velocity models with and without vertical gradients: comparison of triclinic anisotropy with simpler anisotropies. *Seismic Waves in Complex 3-D Structures*, 23, 45–59.

Bucha, V. (2017) Kirchhoff prestack depth migration in simple models with differently rotated elasticity tensor: orthorhombic and triclinic anisotropy. *Journal of Seismic Exploration*, 26, 1–24.

Bucha, V. (2019) Kirchhoff prestack depth scalar migration of complete wave fields in simple inhomogeneous weakly anisotropic velocity models: PP, PS1 and PS2 waves. *Seismic Waves in Complex 3-D Structures*, 29, 19–38.

Bucha, V. and Bulant, P. (Eds.) (2019) SW3D-CD-23 (DVD-ROM). *Seismic Waves in Complex 3-D Structures*, 29, 71–72.

Bulant, P. (1996) Two-point ray tracing in 3-D. *Pure and Applied Geophysics*, 148, 421–447.

Bulant, P. (1999) Two-point ray-tracing and controlled initial-value ray-tracing in 3-D heterogeneous block structures. *Journal of Seismic Exploration*, 8, 57–75.

Bulant, P. and Klimeš, L. (1999) Interpolation of ray-theory travel times within ray cells. *Geophysical Journal International*, 139, 273–282.

Červený, V., Klimeš, L. and Pšenčík, I. (1988) Complete seismic-ray tracing in three-dimensional structures. In: Doornbos, D.J. (Ed.) *Seismological Algorithms*. New York, NY: Academic Press, pp. 89–168.

Gajewski, D. and Pšenčík, I. (1990) Vertical seismic profile synthetics by dynamic ray tracing in laterally varying layered anisotropic structures. *Journal of Geophysical Research*, 95B, 11301–11315.

Gray, S., H., Etgen, J., Dellinger, J. and Whitmore, D. (2001) Seismic migration problems and solutions. *Geophysics*, 66, 1622–1640.

Hokstad, K. (2000) Multicomponent Kirchhoff migration. *Geophysics*, 65, 861–873.

Hou, A. and Marfurt, K. J. (2002) Multicomponent prestack depth migration by scalar wavefield extrapolation. *Geophysics*, 67, 1886–1894.

Klimeš, L. (2002) Relation of the wave-propagation metric tensor to the curvatures of the slowness and ray-velocity surfaces. *Studia Geophysica et Geodaetica*, 46, 589–597.

Kuo J.T and Dai, T. (1984) Kirchhoff elastic wave migration for the case of noncoincident source and receiver. *Geophysics*, 49, 1223–1238.

Mensch, T. and Rasolofosaon, P. (1997) Elastic-wave velocities in anisotropic media of arbitrary symmetry-generalization of Thomsen's parameters ϵ, δ and γ. *Geophysical Journal International*, 128, 43–64.

Qizhen, D. and Bo, H. (2008) Elastic Kirchhoff migration of vectorial wave-fields. *Applied Geophysics*, 5(4), 284–293.

Tessmer, E. (1995) 3-D seismic modeling of general material anisotropy in the presence of the free surface by a Chebychev spectral method. *Geophysical Journal International*, 121, 557–575.

Versteeg, R.J. and Grau, G. (Eds.) (1991) The Marmousi experience. *Proceedings of the EAGE workshop on Practical Aspects of Seismic Data Inversion*. Zeist: European Association of Exploration Geophysicists.

Waheed, U., Psencik, I., Cerveny, V., Iversen, E., and Alkhalifah, T. (2013) Two-point paraxial traveltime formula for inhomogeneous isotropic and anisotropic media: tests of accuracy. *Geophysics*, 78, C41–C56.

Wang, W. and McMechan, G.A. (2016) Vector-based image condition for 3D elastic reverse time migrations. 86th SEG Annual International meeting, Expanded Abstracts, 4168–4172.